



Article

Thin-Film Transistors from Electrochemically Exfoliated In₂Se₃ Nanosheets

Xiangxiang Gao ^{1,2} , Hai-Yang Liu ², Jincheng Zhang ³, Jian Zhu ^{2,*}, Jingjing Chang ^{1,3,*} and Yue Hao ³

¹ Advanced Interdisciplinary Research Center for Flexible Electronics, Xidian University, Xi'an 710071, China; gaoliangxiang@xidian.edu.cn

² National Institute for Advanced Materials, School of Materials Science and Engineering, Nankai University, Tianjin 300350, China; haiyang-l@mail.nankai.edu.cn

³ State Key Discipline Laboratory of Wide Band Gap Semiconductor Technology, School of Microelectronics, Xidian University, Xi'an 710071, China; jchzhang@xidian.edu.cn (J.Z.); yhao@xidian.edu.cn (Y.H.)

* Correspondence: zj@nankai.edu.cn (J.Z.); jjingchang@xidian.edu.cn (J.C.)

Abstract: The wafer-scale fabrication of two-dimensional (2D) semiconductor thin films is the key to the preparation of large-area electronic devices. Although chemical vapor deposition (CVD) solves this problem to a certain extent, complex processes are required to realize the transfer of thin films from the growth substrate to the device substrate, not to mention its harsh reaction conditions. The solution-based synthesis and assembly of 2D semiconductors could realize the large-scale preparation of 2D semiconductor thin films economically. In this work, indium selenide (In₂Se₃) nanosheets with uniform sizes and thicknesses were prepared by the electrochemical intercalation of quaternary ammonium ions into bulk crystals. Layer-by-layer (LbL) assembly was used to fabricate scalable and uniform In₂Se₃ thin films by coordinating In₂Se₃ with poly(diallyldimethylammonium chloride) (PDDA). Field-effect transistors (FETs) made from a single In₂Se₃ flake and In₂Se₃ thin films showed mobilities of 12.8 cm²·V⁻¹·s⁻¹ and 0.4 cm²·V⁻¹·s⁻¹, respectively, and on/off ratios of >10³. The solution self-assembled In₂Se₃ thin films enriches the research on wafer-scale 2D semiconductor thin films for electronics and optoelectronics and has broad prospects in high-performance and large-area flexible electronics.

Keywords: two dimensional semiconductors; layer-by-layer assembly; field-effect transistors



Citation: Gao, X.; Liu, H.-Y.; Zhang, J.; Zhu, J.; Chang, J.; Hao, Y.

Thin-Film Transistors from Electrochemically Exfoliated In₂Se₃ Nanosheets. *Micromachines* **2022**, *13*, 956. <https://doi.org/10.3390/mi13060956>

Academic Editor: Bassem Salem

Received: 27 May 2022

Accepted: 15 June 2022

Published: 16 June 2022

Publisher's Note: MDPI stays neutral with regard to jurisdictional claims in published maps and institutional affiliations.



Copyright: © 2022 by the authors. Licensee MDPI, Basel, Switzerland. This article is an open access article distributed under the terms and conditions of the Creative Commons Attribution (CC BY) license (<https://creativecommons.org/licenses/by/4.0/>).

1. Introduction

Two dimensional semiconductors have promoted the rapid development of electronics and optoelectronic devices due to their excellent charge transport properties and mechanical character [1,2]. The wafer-scale fabrication of well-ordered and uniform 2D semiconductor thin films are indispensable for large-area electronics and crucial to the practical application and development of 2D semiconductors [3–5]. High-quality 2D semiconductor thin films can be grown by chemical vapor deposition (CVD) [5–7]. However, the reaction conditions are stringent, and arduous transferring procedures are required to realize the transfer of thin films from the growth substrates to the targeted substrates. The transfer process is not only cumbersome and time-consuming, but it may also cause irreversible damage to the semiconductor device performance and reduce device yield.

Alternatively, uniform 2D semiconductor thin films can be economically prepared by a solution method from solution-processed 2D semiconductors colloidal inks [8,9]. Solution-processable 2D semiconductor electronics is an emerging research area, and substantial progress has been made. It has been reported that the electrochemical intercalation of quaternary ammonium ions is powerful in preparing stable 2D semiconductor inks such as graphite, black phosphorus, MoS₂, In₂Se₃, and NbSe₂ [10–14]. Their thin films have a wide range of applications in the fields of superconductors, field-effect transistors (FETs), photodetectors, and spin electronics. The spin-coated and LbL-assembled MoS₂ thin films

from electrochemically exfoliated MoS₂ nanosheets used as FETs channels show mobilities of $\approx 10 \text{ cm}^2 \cdot \text{V}^{-1} \cdot \text{s}^{-1}$ and on/off ratios of $>10^5$ [13,15]. Such device performance is superior to other solution-processed 2D semiconductor thin-film devices. The vacuum-filtrated In₂Se₃ thin films with thicknesses of 10 μm show ultrafast response, with rise and decay times of 41 and 39 ms, respectively, and efficient photoresponsivity (1 mA W^{-1}) [16]. However, conventional, solution-based, thin-film deposition approaches confront the problems of uncontrollable film thickness, uneven deposition, and the coffee ring effect.

In this work, we propose LbL assembly as an effective method of fabricating scalable 2D thin films from electrochemically exfoliated nanosheets. LbL assembly is based on the alternating assembly of two species with complementary interactions (such as electrostatic attraction, hydrophobic interactions, or hydrogen bonds) and can prepare thin films, patterns, and heterostructures on any substrate. Various low-dimensional electronic nanofilms, including gold nanoparticles, single-walled carbon nanotubes, boron nitride, clay nanosheets, and MoS₂, have been successfully assembled by LbL assembly with precise thickness control [15,17–21]. Here, we assembled uniform In₂Se₃ thin films by electrostatic adsorption between poly(diallyldimethylammonium chloride) (PDDA) and electrochemically exfoliated In₂Se₃. The single In₂Se₃ flake and LbL-assembled In₂Se₃ thin films, serving as active channel materials in FETs, possessed excellent device performance. The mobility and on/off ratio of the LbL-assembled In₂Se₃ thin films were even better than the CVD-grown In₂Se₃ thin film, showing the robustness of solution-processed electronics.

2. Materials and Methods

2.1. Materials

Bulk In₂Se₃ was purchased from Six Carbon Technology (Shenzhen, China). Tetraheptylammonium bromide (THAB) was purchased from Aladdin (Shanghai, China). Polyvinyl pyrrolidone (PVP) was purchased from Energy Chemical (Shanghai, China). Poly(diallyldimethylammonium chloride) (PDDA) was purchased from Sigma-Aldrich (Shanghai, China). Polyurethane was purchased from Yantai Wanhua Polyurethane Co., Ltd. (Yantai, China). Cr and Au metals were purchased from Vnano Vacuum Technology Co., Ltd. (Beijing, China). Carbon rod was purchased from Tianjin Aida Hengsheng Technology Development Co., Ltd. (Tianjin, China). Other solutions, including Acetonitrile, N,N-Dimethylformamide (DMF), acetone, and ethanol and isopropyl alcohol were purchased from Tianjin Chemical Reagent Company (Tianjin, China). Ultrapure water ($20 \text{ M}\Omega \cdot \text{cm}^{-1}$) was prepared by a Sartorius Arium pro UF system made by Sartorius (Göttingen, Germany).

2.2. Synthesis of In₂Se₃ Nanosheets

In₂Se₃ nanosheets were synthesized by the electrochemical intercalation of quaternary ammonium ions. The electrochemical intercalation was performed in a $5 \text{ mg} \cdot \text{mL}^{-1}$ tetraheptylammonium bromide (THAB) acetonitrile solution, with the bulk In₂Se₃ and carbon rod serving as cathode and anode, respectively. The intercalation voltage was 8 V. After the intercalation, the THAB-intercalated In₂Se₃ was collected and sonicated in a 0.2 M polyvinyl pyrrolidone (PVP) solution (PVP: molecular weight of about 10,000) for 30 min to form a brown dispersion of In₂Se₃ nanosheets. The In₂Se₃ dispersion was subsequently centrifuged and washed with DMF several times to remove excessive PVP. The final In₂Se₃ dispersion was centrifuged at 1000 rpm for 5 min, and precipitates were discarded. The supernatant was concentrated in DMF for characterization and thin-film assembly.

2.3. Fabrication of In₂Se₃ Thin Films

The In₂Se₃ thin films were assembled by LbL assembly. Before LbL assembly, the SiO₂/Si substrates were pre-cleaned with acetone as well as ethanol and isopropyl alcohol. The substrates were treated with oxygen plasma at 100 W for 5 min to produce a superwetting surface. The substrates were firstly immersed in a positively charged PDDA solution (0.1 wt %) for 2 min to deposit single-layer PDDA chains and were then rinsed by

ultrapure water and gently dried with the use of an air gun. The substrates attached with PDDA chains were then immersed in negatively charged In_2Se_3 dispersion for 5 min, and In_2Se_3 nanosheets were assembled in order on the substrates by the electrostatic interaction between the PDDA and In_2Se_3 . Finally, the substrates were rinsed by ultrapure water to remove the loosely attached In_2Se_3 nanosheets and were dried by air gun. The first cycle of the LbL assembly of the In_2Se_3 thin film was then completed. It is worth noting that the concentration of the In_2Se_3 dispersion was monitored by optical absorbance in order to assemble high-quality thin films. The single-layer, assembled In_2Se_3 thin films were dense when the characteristic absorbance at 450 nm was about 0.6 after the In_2Se_3 inks were diluted 500 times.

2.4. Fabrication of In_2Se_3 FETs

The channels of the FETs were fabricated by nanofiber masks. Aligned polyurethane nanofibers, whose diameters were maintained at ~ 500 nm, were printed on the substrates covered by In_2Se_3 single flakes or thin films. Subsequently, metal coatings (5 nm/45 nm Cr/Au) with a $200 \times 200 \mu\text{m}$ metal mask were deposited by thermal evaporation to create source and drain electrodes. Finally, the SiO_2/Si substrates were immersed in the DMF solvent for 30 min and sonicated for 5 min to remove the polyurethane fiber, and the channel of the FET devices could be successfully prepared. In order to improve the contact between the electrode and the In_2Se_3 , the devices were annealed at 200°C in vacuum for 2 h before the test.

3. Results

3.1. Synthesis and Characterizations of In_2Se_3 Nanosheets

In_2Se_3 nanosheets were synthesized by the electrochemical intercalation of quaternary ammonium ions, as shown in Figure 1a. The electrochemical intercalation was performed in a $5 \text{ mg}\cdot\text{mL}^{-1}$ tetraheptylammonium bromide (THAB) acetonitrile solution, with the bulk In_2Se_3 and the carbon rod serving as cathode and anode, respectively. Driven by external voltage, the positively charged THA^+ ions were inserted into the bulk In_2Se_3 and became fluffy and fell off from the cathode. The THAB-intercalated In_2Se_3 were collected and sonicated in a 0.2 M polyvinyl pyrrolidone (PVP) solution (PVP: molecular weight of about 10,000) for 30 min to form a brown dispersion of In_2Se_3 nanosheets (Figure 1b). There is a new XRD peak at a diffraction angle of about 6° in the THAB-intercalated In_2Se_3 , indicating that the interlayer spacing of the THAB-intercalated In_2Se_3 increased from 9.7 \AA to 17 \AA and further proved the successful insertion of the THA^+ ions (Figure 1c). PVP acts as a surfactant to stabilize the In_2Se_3 nanosheet solution and prevent the agglomeration and sedimentation. The excessive PVP was removed by repeatedly washing with N,N-Dimethylformamide (DMF). The final In_2Se_3 dispersion was centrifuged at 1000 rpm for 3 min to sort the nanosheets. The sediments containing unexfoliated layered crystallites were discarded. The supernatant was concentrated in DMF for characterization and thin-film assembly. AFM showed that the exfoliated In_2Se_3 nanosheets had micron-level lateral dimensions (Figure 1d). A total of 90% of the In_2Se_3 nanosheets have thicknesses of 2.2 nm, further confirming the few-layer nature of the In_2Se_3 nanosheets and the uniformity of the thicknesses (Figure 1e). The lamellar structure of the In_2Se_3 nanosheet was verified by a transmission electron microscopy (TEM) image (Figure 2a), and the selected area electron diffraction (SAED) patterns indicated the single crystalline characteristics of the In_2Se_3 nanosheet (Figure 2b). The In 3d and Se 3d binding energy peaks of the electrochemically intercalated In_2Se_3 shifted to higher values as compared with the bulk In_2Se_3 due to the n-type doping induced by the insertion of the THA^+ ions (Figure 2c,d).

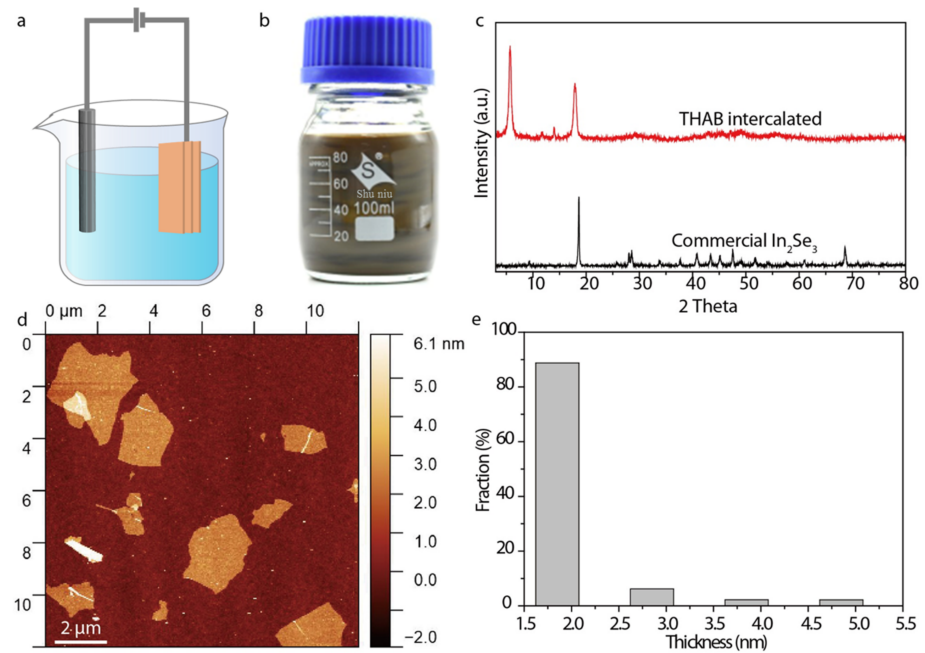


Figure 1. Synthesis and characterizations of In₂Se₃ nanosheets. (a) Schematic of the electrochemical exfoliation of the layered In₂Se₃ into nanosheets. (b) Photograph of In₂Se₃ dispersion in DMF. (c) XRD patterns of the THAB-intercalated bulk In₂Se₃ compared with commercial In₂Se₃. (d) Atomic force microscopy (AFM) image of In₂Se₃ nanosheets. (e) Thickness distribution of In₂Se₃ nanosheets.

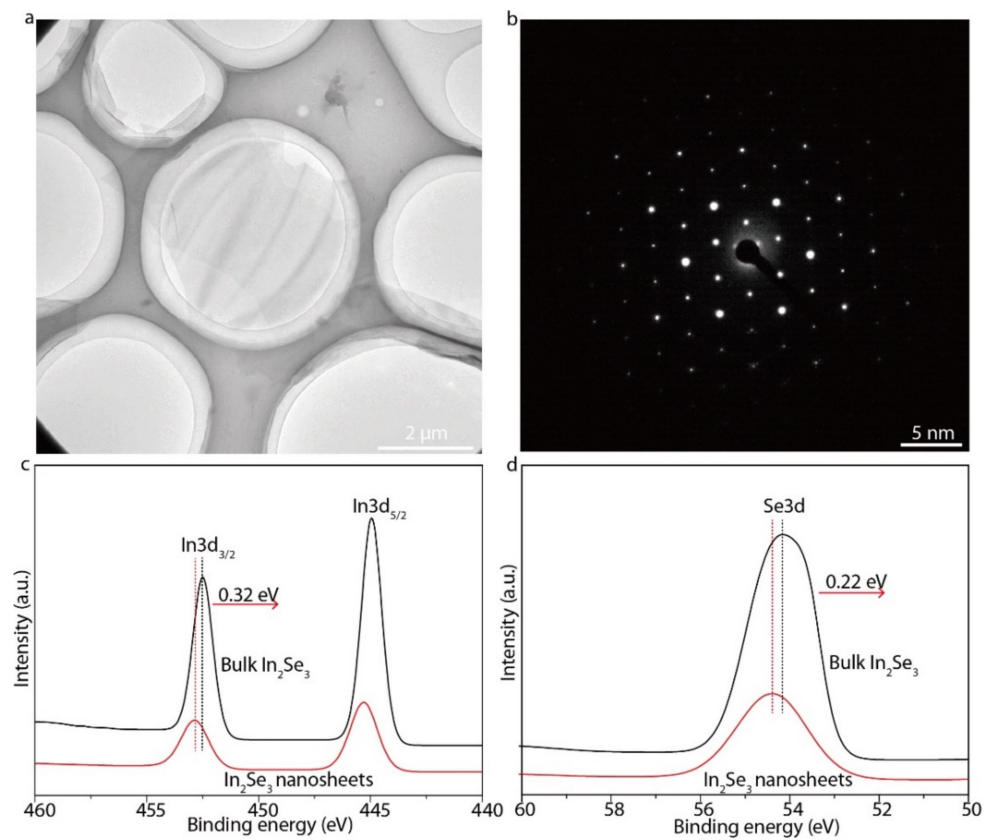


Figure 2. Characterizations of In₂Se₃ nanosheets. (a) TEM image of In₂Se₃ nanosheets. (b) Selected-area electron diffraction image of an In₂Se₃ nanosheet. (c) Comparison of In 3d binding energies of electrochemically intercalated In₂Se₃ nanosheets and bulk In₂Se₃. (d) Comparison of Se 3d binding energies of electrochemically intercalated In₂Se₃ nanosheets and bulk In₂Se₃.

3.2. LbL Assembled In_2Se_3 Thin Films

Well-ordered and uniform 2D semiconductor thin films are of vital importance to device performance. We chose LbL assembly to fabricate In_2Se_3 thin films by sequentially adsorbing the PDDA solution and the In_2Se_3 dispersion on SiO_2/Si substrates through electrostatic interactions (Figure 3a). The zeta potential of the In_2Se_3 dispersion was found to be -18.1 mV (Figure 3b). The intercalation of tetraheptylammonium ions led to the injection of electrons into the In_2Se_3 crystal structures and the slightly negatively charged In_2Se_3 nanosheets [22]. Before LbL assembly, the SiO_2/Si substrates were pre-cleaned with acetone as well as ethanol and isopropyl alcohol and then treated with oxygen plasma at 100 W for 5 min to produce a superwetting surface. The substrates were alternatively immersed in the PDDA solution (0.1 wt %) and the In_2Se_3 dispersion, with rinsing by ultrapure water and drying by air gun after each adsorption. The Raman characteristic peak originating from the $A_1(\text{LO} + \text{TO})$ of the In_2Se_3 thin film were consistent with the bulk In_2Se_3 , while the $A_1(\text{LO})$ phonon mode of the In_2Se_3 thin film exhibited a small shift toward lower wavenumbers arising from the smaller vibration coherence length along the c -axis as a result of the weak van der Waals interaction (Figure 3c). The optical microscope image of the LbL-assembled In_2Se_3 thin film revealed that the nanosheets in a wide range of films were evenly stacked and assembled into homogeneous thin films (Figure 3d). From the local AFM and SEM image of the LbL-assembled In_2Se_3 thin film, we can deduce that the adjacent nanosheets were assembled on the substrate through broad-area, plane-to-plane Van der Waals contacts (Figures 3e and 4). The TEM images of the LbL-assembled In_2Se_3 thin film show that the adjacent nanosheets are stacked tightly together with mixed crystalline lattices on the boundaries and further demonstrate decent interfaces (Figure 5). The number of in-plane grain boundaries in the LbL-assembled 2D semiconductor thin films were greatly reduced and will significantly improve charge transport performance.

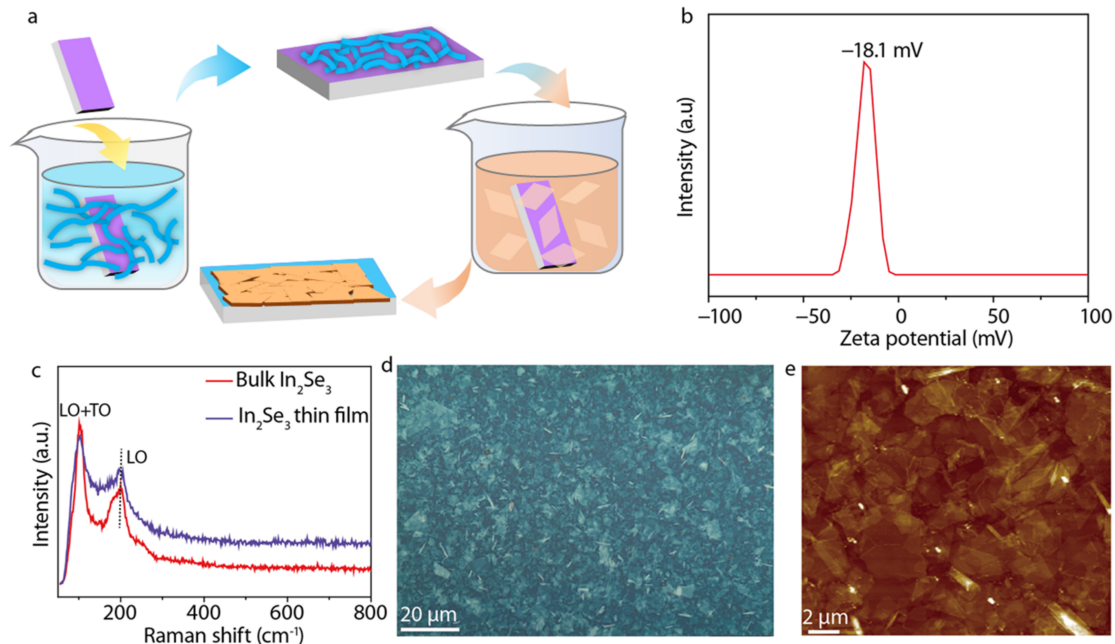


Figure 3. LbL assembly of In_2Se_3 thin films. (a) Schematic of the LbL assembly process. (b) Zeta potential of In_2Se_3 nanosheets dispersed in deionized water. (c) Raman spectra of In_2Se_3 thin films (purple) compared with bulk In_2Se_3 (red). (d) Optical microscope image of LbL-assembled In_2Se_3 thin films. (e) AFM image of LbL-assembled In_2Se_3 thin films.

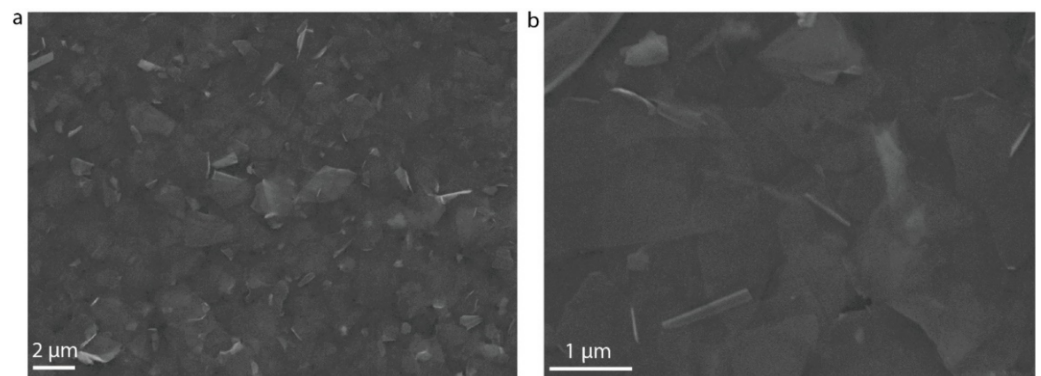


Figure 4. SEM image of LbL-assembled In_2Se_3 thin films at different magnifications. (a) SEM image of LbL-assembled In_2Se_3 thin films with 2 μm scale bar. (b) SEM image of LbL-assembled In_2Se_3 thin films with 1 μm scale bar.

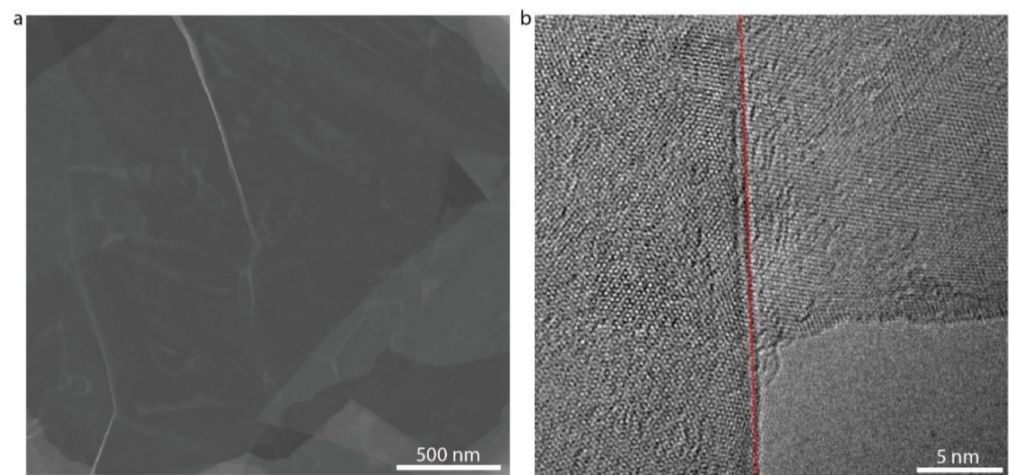


Figure 5. TEM image of LbL-assembled In_2Se_3 thin films. (a) Low-resolution TEM image of the LbL-assembled In_2Se_3 thin films. (b) High-resolution TEM image of the contact region between lateral nanosheets (The red dotted line is the edge of a nanosheet. The right shows the lattice of a single nanosheet, and the left shows the lattice of stacked nanosheets).

3.3. Performance of FETs from Electrochemically Exfoliated In_2Se_3 Nanosheets

To investigate the electric properties of solution-processed In_2Se_3 , we further prepared In_2Se_3 single-flake and In_2Se_3 thin-film FETs on a 300 nm SiO_2/Si substrate. The channels of the FETs were fabricated by nanofiber masks (Figure 6) [23]. First, we used the diluted and concentrated In_2Se_3 dispersion to adsorb the sparse In_2Se_3 nanosheets and dense In_2Se_3 thin films on a pre-treated SiO_2/Si substrate by LbL assembly. Then, polyurethane nanofibers were printed and metal electrodes were deposited in order to fabricate FET devices. Figure 7a shows the scanning electron microscope (SEM) image of the In_2Se_3 single-flake FET with a length of 506 nm and an average width of 600 nm. The In_2Se_3 single-flake is perfectly flat on the channel to ensure good contact between the electrode and the In_2Se_3 nanosheet. The $I_{\text{sd}}-V_{\text{sd}}$ output characteristics of the In_2Se_3 single-flake FET showed a linear trend, indicating ohmic contacts between the In_2Se_3 single-flake and electrode (Figure 7b). The forward and reverse $I_{\text{sd}}-V_{\text{g}}$ transfer characteristics of the In_2Se_3 single-flake FET showed a typical n-type behavior with an on/off ratio of 1.5×10^3 at $V_{\text{sd}} = 1 \text{ V}$ (Figure 7c). The electron mobility of individual In_2Se_3 nanosheets can be calculated to be $12.8 \text{ cm}^2 \text{ V}^{-1} \text{ s}^{-1}$ from the linear-regime transfer characteristics using the following equation:

$$\mu = \frac{dI_{\text{sd}}}{dV_{\text{g}}} \times \frac{L}{WC_s V_{\text{sd}}}$$

where L and W are the channel length and width, and C_s is the areal capacitance of 300 nm SiO_2/Si . The channel length and width of the In_2Se_3 thin film FET device are 549 nm and 200 μm , respectively (Figure 7d). The $I_{\text{sd}}-V_{\text{sd}}$ output characteristics of the In_2Se_3 thin film FET exhibited non-linear dependence on V_{sd} due to the pinch-off effect of the FET channel (Figure 7e). The electron mobility of In_2Se_3 thin films reached $0.2 \text{ cm}^2 \text{ V}^{-1} \text{ s}^{-1}$, with an on/off ratio of 7×10^4 at $V_{\text{sd}} = 1 \text{ V}$ (Figure 7f). The carrier mobility of the In_2Se_3 single flake is much higher than that of the In_2Se_3 thin film due to the sheet-to-sheet contact resistance, and the device performance may average out in the percolating thin films. The observed clockwise hysteresis in the transfer characteristics of the In_2Se_3 single-flake and thin-film FETs was attributed to charge trapping and detrapping at the interface between the In_2Se_3 and the SiO_2 (Figure 7c,f) [24]. To further understand the relative effects of PDDA, the spin-coated In_2Se_3 thin-film FETs were fabricated. The doping of the PDDA caused the positive shift of the threshold voltage and the lower maximum on-current as compared with the spin-coated In_2Se_3 thin-film FET (Figure 8a,b).

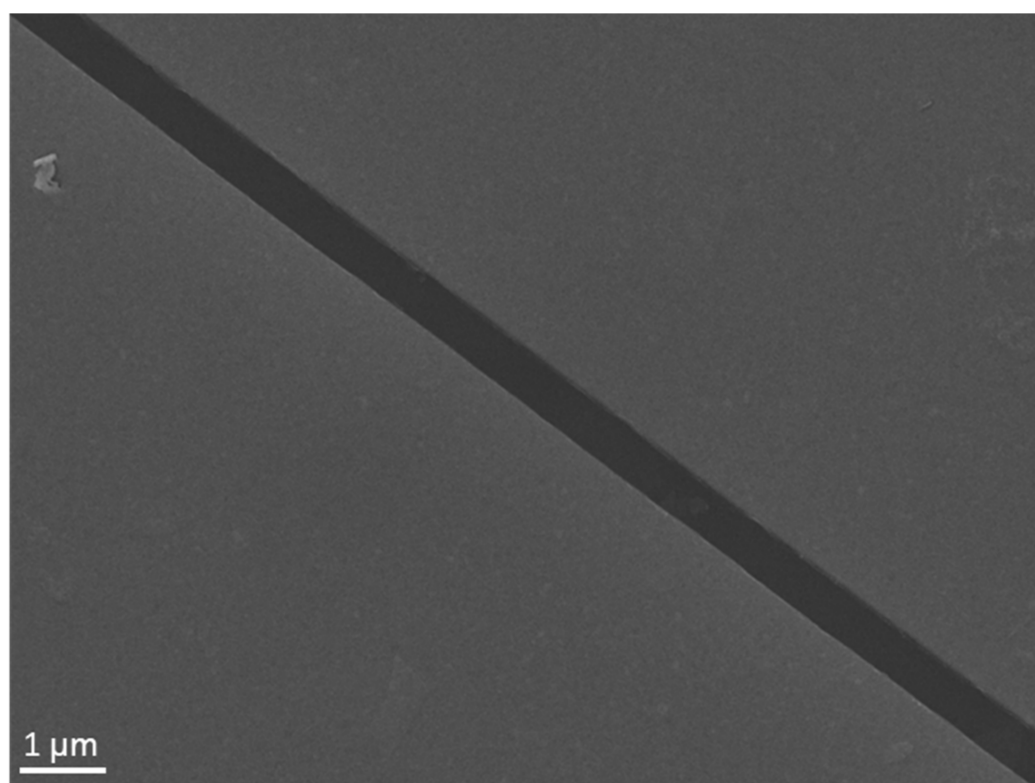


Figure 6. SEM image of the channel fabricated by nanofiber masks.

The performance of electrochemically exfoliated In_2Se_3 single-flake and thin-film FETs were comparable to those made from other methods in terms of mobilities and on/off ratios (Table 1) [25–29]. A comprehensive comparison is provided in Table 1. The electrochemically exfoliated In_2Se_3 single-flake FET performance was superior to some mechanically exfoliated In_2Se_3 flake FETs [27]. The electron mobilities and on/off ratios of the LbL-assembled In_2Se_3 thin film was close to those of the spin-coated In_2Se_3 thin films and CVD-grown In_2Se_3 thin films [12,28]. The outstanding device performances of both single flakes and thin films are attributed to the high-quality nanosheets with uniform sizes and thicknesses prepared by electrochemical intercalation.

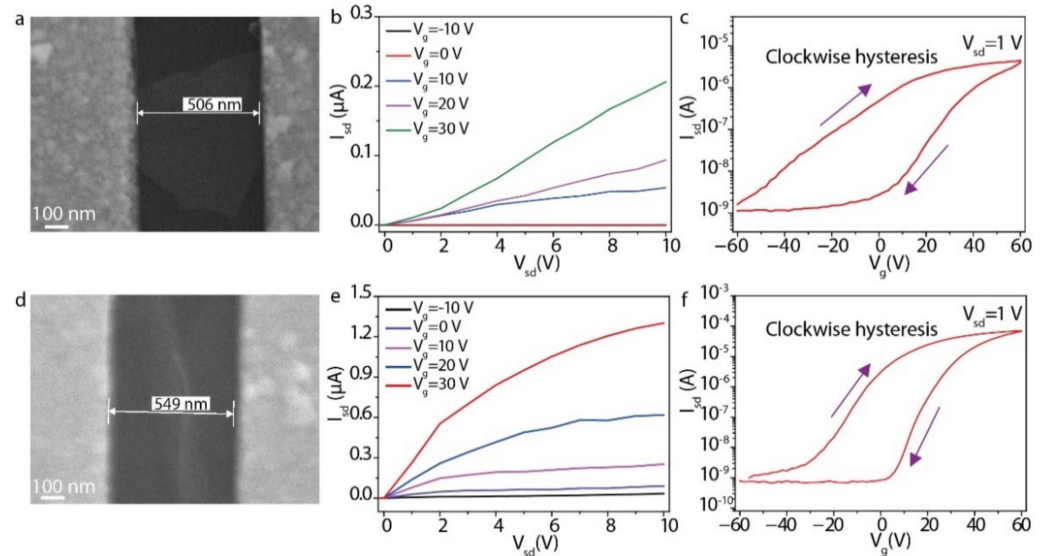


Figure 7. Transistor performance of In_2Se_3 . (a) SEM image of the In_2Se_3 single-flake FET with a single In_2Se_3 nanosheet as the FET channel. (b) $I_{sd}-V_{sd}$ output characteristics of the In_2Se_3 single-flake FET. (c) $I_{sd}-V_g$ transfer characteristics of the In_2Se_3 single-flake FET. (d) SEM image of the In_2Se_3 thin-film FET channel. (e) $I_{sd}-V_{sd}$ output characteristics of the In_2Se_3 thin-film FET. (f) $I_{sd}-V_g$ transfer characteristics of the In_2Se_3 thin-film FET.

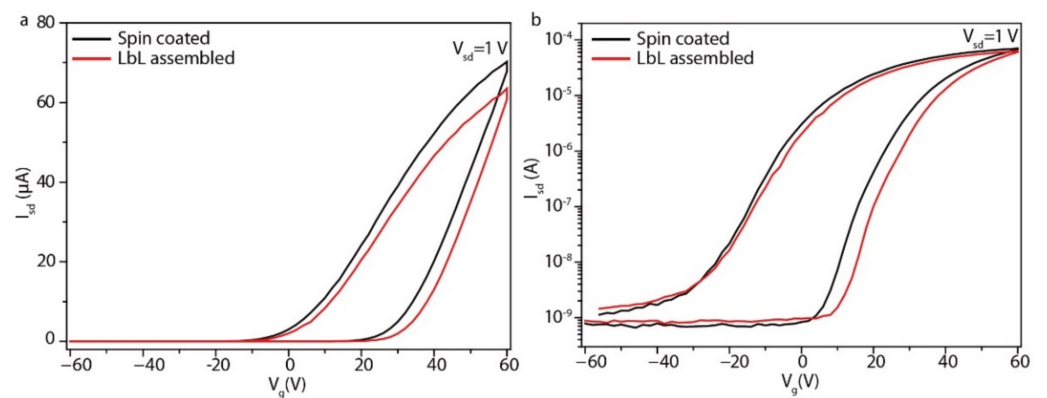


Figure 8. (a) $I_{sd}-V_{sd}$ transfer characteristics of the LbL-assembled and spin-coated In_2Se_3 thin film FETs on a linear scale. (b) $I_{sd}-V_{sd}$ transfer characteristics of the LbL-assembled and spin-coated In_2Se_3 thin film FETs on a logarithmic scale.

Table 1. Comparison of In_2Se_3 FET performance with different preparation methods.

Preparation Methods	Mobility ($\text{cm}^2 \text{V}^{-1} \text{s}^{-1}$)	On/Off Ratio	Reference
Mechanically exfoliated In_2Se_3 flake	30	10^5	[25]
Mechanically exfoliated In_2Se_3 flake	1.26	500	[27]
CVD-grown In_2Se_3 thin film	2.51×10^{-3}	12	[26]
CVD-grown In_2Se_3 thin film	1	10^3	[28]

Table 1. Cont.

Preparation Methods	Mobility ($\text{cm}^2 \text{V}^{-1} \text{s}^{-1}$)	On/Off Ratio	Reference
PVD-grown p type In_2Se_3 flake	2.5	10^3	[29]
Spin-coated In_2Se_3 thin film	0.2	10^5	[12]
Electrochemically exfoliated In_2Se_3 flake	12.8	1.5×10^3	This work
LbL-assembled In_2Se_3 thin film	0.4	7×10^4	

4. Conclusions

In conclusion, we prepared high-quality In_2Se_3 nanosheets through an electrochemical intercalation approach. Homogeneous In_2Se_3 thin films were assembled by the alternate adsorption of PDDA and a nanosheet solution, driven by electrostatic attraction. FETs from solution-processed In_2Se_3 single flakes and thin films showed satisfying performance and were comparable to those from CVD-grown In_2Se_3 thin films, mechanically exfoliated In_2Se_3 flakes, and spin-coated In_2Se_3 thin films. LbL-assembled 2D semiconductor thin films are promising candidates for emerging large-area, flexible, and wearable electronic applications.

Author Contributions: Conceptualization, X.G. and J.Z. (Jian Zhu); methodology, X.G. and H.-Y.L.; software, J.Z. (Jian Zhu); validation, X.G. and J.Z. (Jian Zhu); formal analysis, X.G. and J.Z. (Jian Zhu); investigation, X.G. and H.-Y.L.; resources, J.Z. (Jian Zhu) and J.C.; data curation, H.-Y.L.; writing—original draft preparation, X.G.; writing—review and editing, J.Z. (Jian Zhu) and J.C.; visualization, X.G.; supervision, J.Z. (Jian Zhu) and J.C.; project administration, J.Z. (Jincheng Zhang) and Y.H.; funding acquisition, J.Z. (Jian Zhu), J.C., J.Z. (Jincheng Zhang) and Y.H. All authors have read and agreed to the published version of the manuscript.

Funding: This work was supported by the National Natural Science Foundation of China (Grant Nos. 51873088, 12004195, 61704131, 61804111), by the National Key Research and Development Program of China (Grant Nos. 2021YFA0715600, 2018YFB2202900), by Tianjin Municipal Science and Technology Commission (Grant Nos. 18JCZDJC38400, 20JCQNJC01820, 18ZLZXZF00480), and by Fundamental Research Funds for the Central Universities (Grant No. XJS222212).

Data Availability Statement: The data used to support the findings of this study are available from the corresponding author upon request.

Conflicts of Interest: The authors declare no conflict of interest.

References

- Liu, C.; Chen, H.; Wang, S.; Liu, Q.; Jiang, Y.-G.; Zhang, D.W.; Liu, M.; Zhou, P. Two-dimensional materials for next-generation computing technologies. *Nat. Nanotechnol.* **2020**, *15*, 545–557. [[CrossRef](#)] [[PubMed](#)]
- Wang, Q.H.; Kalantar-Zadeh, K.; Kis, A.; Coleman, J.N.; Strano, M.S. Electronics and optoelectronics of two-dimensional transition metal dichalcogenides. *Nat. Nanotechnol.* **2012**, *7*, 699–712. [[CrossRef](#)] [[PubMed](#)]
- Lin, Z.; McCreary, A.; Briggs, N.; Subramanian, S.; Zhang, K.H.; Sun, Y.F.; Li, X.F.; Borys, N.J.; Yuan, H.T.; Fullerton-Shirey, S.K.; et al. 2D materials advances: From large scale synthesis and controlled heterostructures to improved characterization techniques, defects and applications. *2D Mater.* **2016**, *3*, 042001. [[CrossRef](#)]
- Chen, X.; Xie, Y.; Sheng, Y.; Tang, H.; Wang, Z.; Wang, Y.; Wang, Y.; Liao, F.; Ma, J.; Guo, X.; et al. Wafer-scale functional circuits based on two dimensional semiconductors with fabrication optimized by machine learning. *Nat. Commun.* **2021**, *12*, 5953. [[CrossRef](#)] [[PubMed](#)]
- Li, T.; Guo, W.; Ma, L.; Li, W.; Yu, Z.; Han, Z.; Gao, S.; Liu, L.; Fan, D.; Wang, Z.; et al. Epitaxial growth of wafer-scale molybdenum disulfide semiconductor single crystals on sapphire. *Nat. Nanotechnol.* **2021**, *16*, 1201–1207. [[CrossRef](#)] [[PubMed](#)]
- Li, N.; Wang, Q.; Shen, C.; Wei, Z.; Yu, H.; Zhao, J.; Lu, X.; Wang, G.; He, C.; Xie, L.; et al. Large-scale flexible and transparent electronics based on monolayer molybdenum disulfide field-effect transistors. *Nat. Electron.* **2020**, *3*, 711–717. [[CrossRef](#)]
- Zhou, J.; Lin, J.; Huang, X.; Zhou, Y.; Chen, Y.; Xia, J.; Wang, H.; Xie, Y.; Yu, H.; Lei, J.; et al. A library of atomically thin metal chalcogenides. *Nature* **2018**, *556*, 355–361. [[CrossRef](#)]

8. Gao, X.; Bian, G.; Zhu, J. Electronics from solution-processed 2D semiconductors. *J. Mater. Chem. C* **2019**, *7*, 12835–12861. [[CrossRef](#)]
9. Lin, Z.; Huang, Y.; Duan, X. Van der Waals thin-film electronics. *Nat. Electron.* **2019**, *2*, 378–388. [[CrossRef](#)]
10. Zhang, Y.; Xu, Y. Simultaneous electrochemical dual-electrode exfoliation of graphite toward scalable production of high-quality graphene. *Adv. Funct. Mater.* **2019**, *29*, 1902171. [[CrossRef](#)]
11. Wang, N.; Mao, N.; Wang, Z.; Yang, X.; Zhou, X.; Liu, H.; Qiao, S.; Lei, X.; Wang, J.; Xu, H.; et al. Electrochemical delamination of ultralarge few-layer black phosphorus with a hydrogen-free intercalation mechanism. *Adv. Mater.* **2020**, *33*, 2005815. [[CrossRef](#)] [[PubMed](#)]
12. Lin, Z.; Wan, Z.; Song, F.; Huang, B.; Jia, C.; Qian, Q.; Kang, J.S.; Wu, Y.; Yan, X.; Peng, L.; et al. High-yield exfoliation of 2D semiconductor monolayers and reassembly of organic/inorganic artificial superlattices. *Chem* **2021**, *7*, 1887–1902. [[CrossRef](#)]
13. Lin, Z.; Liu, Y.; Halim, U.; Ding, M.; Liu, Y.; Wang, Y.; Jia, C.; Chen, P.; Duan, X.; Wang, C.; et al. Solution-processable 2D semiconductors for high-performance large-area electronics. *Nature* **2018**, *562*, 254–258. [[CrossRef](#)] [[PubMed](#)]
14. Li, J.; Song, P.; Zhao, J.; Vaklinova, K.; Zhao, X.; Li, Z.; Qiu, Z.; Wang, Z.; Lin, L.; Zhao, M.; et al. Printable two-dimensional superconducting monolayers. *Nat. Mater.* **2020**, *20*, 181–187. [[CrossRef](#)] [[PubMed](#)]
15. Gao, X.; Yin, J.; Bian, G.; Liu, H.-Y.; Wang, C.-P.; Pang, X.-X.; Zhu, J. High-mobility patternable MoS₂ percolating nanofilms. *Nano Res.* **2021**, *14*, 2255–2263. [[CrossRef](#)]
16. Shi, H.; Li, M.; Shaygan Nia, A.; Wang, M.; Park, S.; Zhang, Z.; Lohe, M.R.; Yang, S.; Feng, X. Ultrafast electrochemical synthesis of defect-free In₂Se₃ flakes for large-area optoelectronics. *Adv. Mater.* **2020**, *32*, 1907244. [[CrossRef](#)]
17. Kim, Y.; Zhu, J.; Yeom, B.; Di Prima, M.; Su, X.; Kim, J.-G.; Yoo, S.J.; Uher, C.; Kotov, N.A. Stretchable nanoparticle conductors with self-organized conductive pathways. *Nature* **2013**, *500*, 59–64. [[CrossRef](#)]
18. Wu, J.; Antaris, A.; Gong, M.; Dai, H. Top-down patterning and self-assembly for regular arrays of semiconducting single-walled carbon nanotubes. *Adv. Mater.* **2014**, *26*, 6151–6156. [[CrossRef](#)]
19. Zhu, J.; Liu, X.; Geier, M.L.; McMorrow, J.J.; Jariwala, D.; Beck, M.E.; Huang, W.; Marks, T.J.; Hersam, M.C. Layer-by-Layer assembled 2D montmorillonite dielectrics for solution-processed electronics. *Adv. Mater.* **2016**, *28*, 63–68. [[CrossRef](#)]
20. Zhu, J.; Kang, J.; Kang, J.; Jariwala, D.; Wood, J.D.; Seo, J.-W.T.; Chen, K.-S.; Marks, T.J.; Hersam, M.C. Solution-processed dielectrics based on thickness-sorted two-dimensional hexagonal boron nitride nanosheets. *Nano Lett.* **2015**, *15*, 7029–7036. [[CrossRef](#)]
21. Richardson, J.J.; Björnmalm, M.; Caruso, F. Technology-driven layer-by-layer assembly of nanofilms. *Science* **2015**, *348*, 2491–2501. [[CrossRef](#)] [[PubMed](#)]
22. Wang, C.; He, Q.; Halim, U.; Liu, Y.; Zhu, E.; Lin, Z.; Xiao, H.; Duan, X.; Feng, Z.; Cheng, R.; et al. Monolayer atomic crystal molecular superlattices. *Nature* **2018**, *555*, 231–236. [[CrossRef](#)] [[PubMed](#)]
23. Liu, H.-Y.; Yin, J.; Gao, X.; Zhao, S.; Bian, G.; Li, J.; Wang, C.-P.; Zhu, J. Scalable submicron channel fabrication by suspended nanofiber lithography for short-channel field-effect transistors. *Adv. Funct. Mater.* **2021**, *32*, 2109254. [[CrossRef](#)]
24. Guo, Y.; Wei, X.; Shu, J.; Liu, B.; Yin, J.; Guan, C.; Han, Y.; Gao, S.; Chen, Q. Charge trapping at the MoS₂-SiO₂ interface and its effects on the characteristics of MoS₂ metal-oxide-semiconductor field effect transistors. *Appl. Phys. Lett.* **2015**, *106*, 103109. [[CrossRef](#)]
25. Island, J.O.; Blanter, S.I.; Buscema, M.; van der Zant, H.S.J.; Castellanos-Gomez, A. Gate controlled photocurrent generation mechanisms in high-gain In₂Se₃ phototransistors. *Nano Lett.* **2015**, *15*, 7853–7858. [[CrossRef](#)]
26. Mukherjee, S.; Dutta, D.; Mohapatra, P.K.; Dezanashvili, L.; Ismach, A.; Koren, E. Scalable integration of coplanar heterojunction monolithic devices on two-dimensional In₂Se₃. *ACS Nano* **2020**, *14*, 17543–17553. [[CrossRef](#)]
27. Feng, W.; Gao, F.; Hu, Y.; Dai, M.; Liu, H.; Wang, L.; Hu, P. Phase-engineering-driven enhanced electronic and optoelectronic performance of multilayer In₂Se₃ nanosheets. *ACS Appl. Mater. Interfaces* **2018**, *10*, 27584–27588. [[CrossRef](#)]
28. Feng, W.; Gao, F.; Hu, Y.; Dai, M.; Li, H.; Wang, L.; Hu, P. High-performance and flexible photodetectors based on chemical vapor deposition grown two-dimensional In₂Se₃ nanosheets. *Nanotechnology* **2018**, *29*, 445205. [[CrossRef](#)]
29. Zhou, J.; Zeng, Q.; Lv, D.; Sun, L.; Niu, L.; Fu, W.; Liu, F.; Shen, Z.; Jin, C.; Liu, Z. Controlled synthesis of high-quality monolayered α -In₂Se₃ via physical vapor deposition. *Nano Lett.* **2015**, *15*, 6400–6405. [[CrossRef](#)]